Noise-induced resistance broadening in resistive switching memory (RRAM) - Part II: Array statistics

Stefano Ambrogio, *Student Member, IEEE*, Simone Balatti, *Student Member, IEEE*, Vincent McCaffrey, Daniel Wang, Daniele Ielmini, *Senior Member, IEEE*

I. Introduction

Resistive switching memory (RRAM) [2] and conductive-bridge RAM (CBRAM) [3]–[5] are attracting a wide interest due to their good performance in terms of low-power consumption [6], speed [7], [8], and endurance [9], [10]. Due to its filamentary switching and conduction, however, RRAM and CBRAM (RRAM will be used to indicate both technologies in the following) are affected by current noise and the related broadening of resistance levels [1], [11]. Noise appears generally as a $1/f$ fluctuation of the current, which can be understood by the superposition of several individual components of random telegraph noise (RTN) [1]. It was shown that the programmed resistance controls the amplitude of both RTN [12], [13] and $1/f$ noise [1] via size-dependent carrier depletion in the conductive filament (CF) or, more generally, the conduction path. Due to the atomistic size of the conduction path in the high resistance state (HRS), a larger noise is found in HRS compared to the low resistance state (LRS) [1]. While a good understanding was established for $1/f$ noise and RTN in typical cells, the statistical distribution of noise and the giant noise phenomena contributing to distribution tail are still elusive.

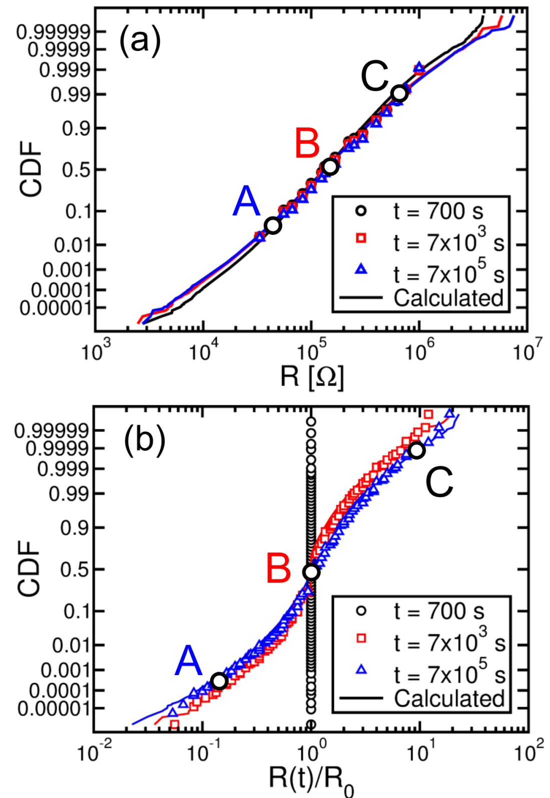

Fig. 1. Measured and calculated distributions of R (a) and of $R(t)/R_0$ (b) for increasing times 700 s, 7x10^3 s and 7x10^5 s. Note the increasing tails in (b) due to current fluctuations. Selected cells A, B and C are also shown in their final position within the distributions at t = 7x10^5 s.

This work addresses noise in a RRAM array by studying the resistance fluctuation and its distributions within the array. We find that resistance broadening is mainly caused by 2 phenomena, namely (i) random walk (RW) consisting of step changes of resistance at random time and amplitude, and (ii) intermittent RTN, where the random 2-level fluctuation randomly starts and stops in the RRAM cell. RW shows a time-dependent fluctuation that gradually stabilizes after device reset. Based on physically-based descriptions of RW and interrupted RTN, we develop a numerical Monte-Carlo model to predict the resistance broadening in the array. The model is applied to RRAM arrays with 2 different metal oxides in the switching layer, evidencing the universal role of RW

S. Ambrogio, S. Balatti and D. Ielmini are with the Dipartimento di Elettronica, Informazione e Bioingegneria and Italian Universities Nanoelectronics Team (IU.NET), Politecnico di Milano, piazza L. da Vinci 32, 20133 Milano, Italy. E-mail: daniele.ielmini@polimi.it. V. McCaffrey and D. Wang are with Adesto Technologies, Sunnyvale, California, USA.

and interrupted RTN in controlling the noise performance in RRAM materials and devices.

A preliminary study on noise-induced broadening of resistance in RRAM arrays was reported in [11]. In this work, we extend the analysis of [11] by describing the statistical distribution of RW events and fluctuating defects among the cells in the array, thus providing a deeper insight into the fluctuation physics of RW and RTN.

II. RRAM DEVICES AND CHARACTERISTICS

Measurements were performed on RRAM arrays with one-transistor/one-resistor (1T1R) structure. The resistor element consisted in a RRAM device composed by a Cu-containing active-metal top electrode, an inert bottom electrode and a metal-oxide switching layer. Two different metal oxides were used in this work, which we refer to as stack A and B in the following. All measurements were carried out on stack A, except where noted. Devices in the array were first programmed in the HRS, where noise is maximum [14], [15] then the read current I_{read} of each device was measured at V_{read} = 0.1 V every 700 s by an on-chip comparator capable of recognizing the resistance R within 17 discrete bins, from 33.3 kΩ to 1 MΩ. Resistance values below 33.3 kΩ and above 1 MΩ could not be measured. The entire measurement lasted a total time of 7x10^5 s, i.e. approximately 8 days.

III. TIME EVOLUTION OF R DISTRIBUTIONS

Fig. 1a shows the cumulative distribution function (CDF) of the measured R for a 512 kbit RRAM sub-array at increasing times t = 7x10^2 s (first measurement point), 7x10^3 s and 7x10^5 s (final measurement point). The distribution is truncated at 33.3 kΩ and 1 MΩ due to the limitations of our on-chip readout scheme. The distribution shows a relatively large spread already at 7x10^2 s and the broadening at increasing time appears negligible. No drift of resistance can also be noticed from these data, evidencing the good data retention of HRS. To better investigate resistance fluctuations in the CDF of Fig. 1a, we analyzed the ratio $R(t)/R_0$ between the resistance of a RRAM device at a generic time t and the initial resistance of the same device at 7x10^2 s. The resulting CDF is reported in Fig. 1b at increasing times. Initially the CDF shows zero standard deviation, since all R values, divided by their initial value, give the same result, namely R(7x10^2 s)/R_0 = 1. Then the CDF broadens with two symmetrical tails for t = 7x10^3 s, followed by a further slight increase of the broadening for t = 7x10^5 s. From the comparison of the results in Figs. 1a and b, we conclude that the distribution in Fig. 1a cannot evidence any resistance fluctuation, due to the dynamic equilibrium of noise where, for any increasing resistance, another R decreases. Therefore, we used the CDF of the normalized $R(t)/R_0$ in Fig. 1b to monitor the resistance fluctuations to either relatively high or low values in correspondence of the two distribution tails.

To highlight the resistance fluctuations, Fig. 2 shows the measured R for 3 cells A, B and C whose final positions in the CDF at 7x10^5 s are reported in Fig. 1. All cells show an initial resistance of about 150 kΩ, in correspondence of the median of the CDF in Fig. 1a. Cell A represents a tail cell where the final resistance is relatively low, while cell B shows a relatively stable resistance from the beginning to the end of the experiment. Finally, cell C shows an increase to a relatively high final resistance. Fig. 2 shows that the resistance mainly changes by random steps, a behavior that we will refer to as *random walk* (RW) where individual RW events appear at times t_{RW}. RTN fluctuations also appear, although generally showing activity only for time periods of length t_{on}.

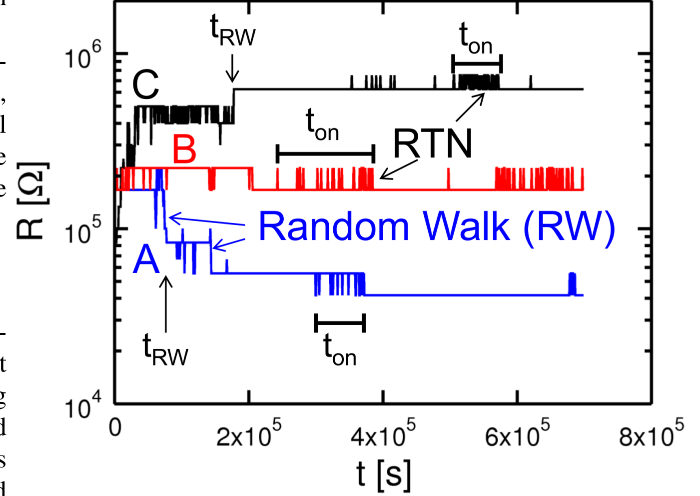

Fig. 2. Measured R as a function of time for cells A, B and C in Fig. 1, showing RW occurring at t_{RW} and interrupted RTN lasting for time t_{on}.

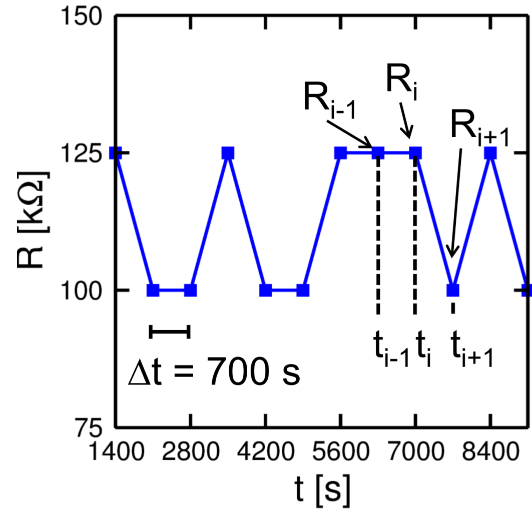

Fig. 3. Measured R as a function of time, indicating the definition of read resistance R_{i-1} and R_i at time t_{i-1} and t_i, respectively.

IV. ANALYSIS OF R FLUCTUATIONS

Fig. 3 shows an example of the measured R as a function of time, where each R sample is collected at time values separated by a sampling time Δt = 700 s. In the figure, we define consecutive values of resistance R_{i-1}, R_i and R_{i+1}, measured at times t_{i-1}, t_i and t_{i+1}, where i is a generic integer i > 1. From Fig. 3, we can define the relative amplitude of

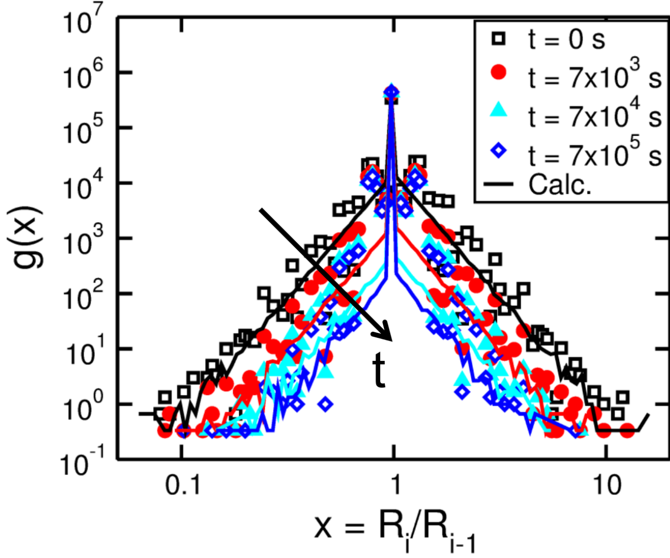

Fig. 4. Measured and calculated distribution $g(x)$ of relative steps $x = R_i/R_{i-1}$ at increasing times. The distributions display symmetric tails with slope $g(x) \sim x^{\pm 4.5}$ which decrease with observation time.

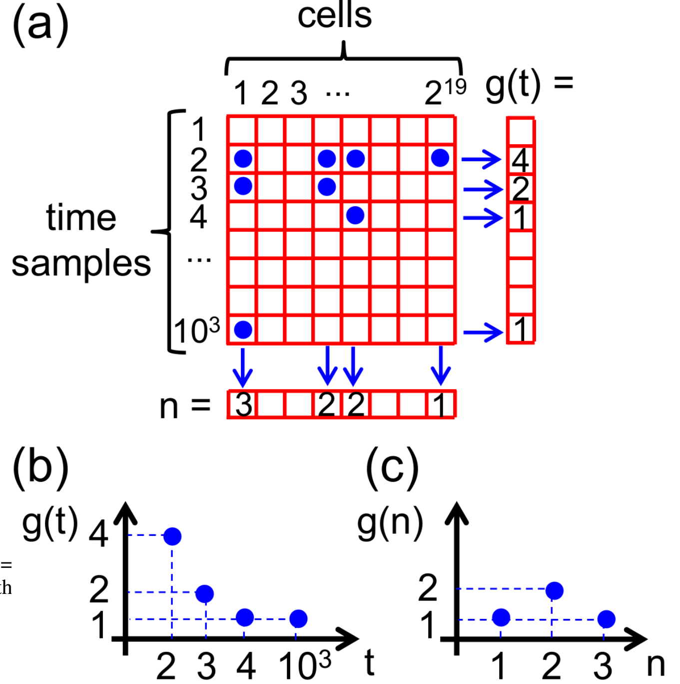

Fig. 5. Schematic illustration of the extraction of the distributions $g(t)$ of the number of events at time t, and $g(n)$ of the number of cells displaying n events in the whole measurement time. An event is defined as a resistance step change above a given x, or below $1/x$.

a resistance step x at time t_i as the ratio between R_i and resistance R_{i-1} at previous time step t_{i-1}, namely:

$$x = \frac{R_i}{R_{i-1}}. \tag{1}$$

A. Distribution of step amplitude

Fig. 4 shows the distribution $g(x)$ of the relative step x for all array devices at times t_i = 1400 s, 7x10^3 s, 7x10^4 s and 7x10^5 s. At any time, $g(x)$ shows a symmetric shape on the bilogarithmic scale, revealing that resistance steps are equally probable toward higher or lower resistance. The high and low tails of $g(x)$ display a power-law behavior described by:

$$g(x) \propto (x)^{\pm 4.5}, \tag{2}$$

where + and - applies to the low- and high-x tails, respectively. At x = 1, the distribution peaks around 10^6 which is the number of cells with no resistance change in the time step considered. While the slope of $g(x)$ remains approximately constant at increasing time, the amplitude of tails decreases, indicating that steps with relatively large amplitude become increasingly less probable with time. This result indicates that RRAM fluctuations decay with time, thus cannot be explained by any stationary model of noise, such as the standard $1/f$ noise or RTN.

B. Distribution of time and number of events

To further study the time decay of fluctuations in Fig. 4, 2 distributions were defined, as schematically shown in Fig. 5. This is a representation of the step events, where each event corresponds to a step of normalized height R$_i$/R$_{i-1}$ higher than x or lower than $1/x$, as a function of the cell number (x-axis) and time (y-axis). Therefore, each box in the array of Fig. 5a corresponds to a cell (from 1 to 2^{19}, corresponding to the 0.5 Mb sub-array in our experiment) at a given time (from 1 to 10^3). A dot in a box corresponds to an event, namely a resistance change above the threshold occurring in a cell at a certain time sample. We define the time distribution of events $g(t)$, shown at the right side of Fig. 5a, as the number of events occurring at time t, *e.g.*, 4 steps are seen in the whole sub-array in correspondence of the 2nd sample in Fig. 5, hence $g(t)$ = 4 for that time sample. On the other hand, the step-number distribution $g(n)$, shown at the bottom side of Fig. 5a, counts the number of cells showing n steps in the whole measurement. For instance, only one cell displays 3 events in Fig. 5, therefore $g(n = 3)$ = 1. Fig. 5b and c schematically show the distribution $g(t)$ and $g(n)$, respectively, corresponding to the time/cell distribution of events in Fig. 5a.

Fig. 6 shows the extracted $g(t)$ for different thresholds of step amplitude x > 2, 3, 4, 5. Each distribution $g(t)$ in the figure includes both steps to higher resistance above a certain amplitude (e.g., x = R$_i$/R$_{i-1}$ > 5) and steps to lower resistance above the same amplitude in the bilogarithmic scale (e.g., x < 1/5), as also assumed in Fig. 5. This allows to consider both left and right tails in the symmetric distribution $g(x)$ in Fig. 4. All distributions show an initial decrease with a slope of -1, followed by a saturated region which lasts until the end of the measurement. We found that the initial decaying behavior, which is consistent with the decay of $g(x)$ in Fig. 4, can be attributed to RW steps which are increasingly less frequent as the time increases from the reset pulse. The decrease of

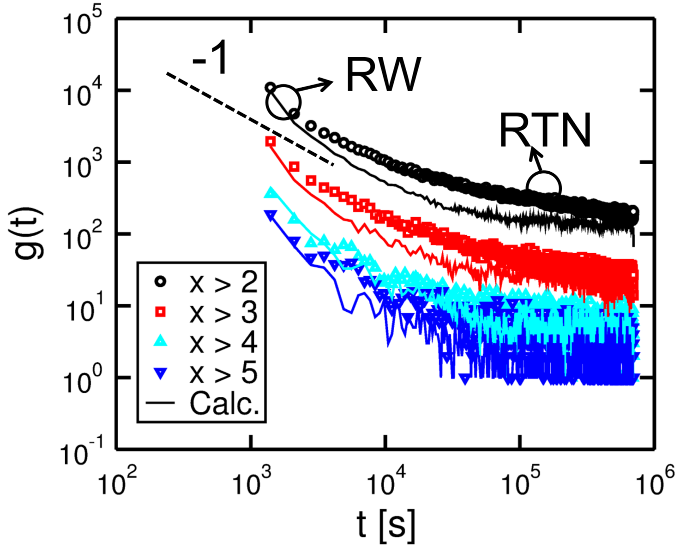

Fig. 6. Measured and calculated $g(t)$ for x > 2,3,4,5. Each distribution also includes events of resistance decrease with R < 1/2, 1/3, 1/4 and 1/5, respectively. Time-dependent RW dominates at short times where $g(t)$ displays a slope equal to -1, while RTN contributes mainly in the the saturated regime at long times.

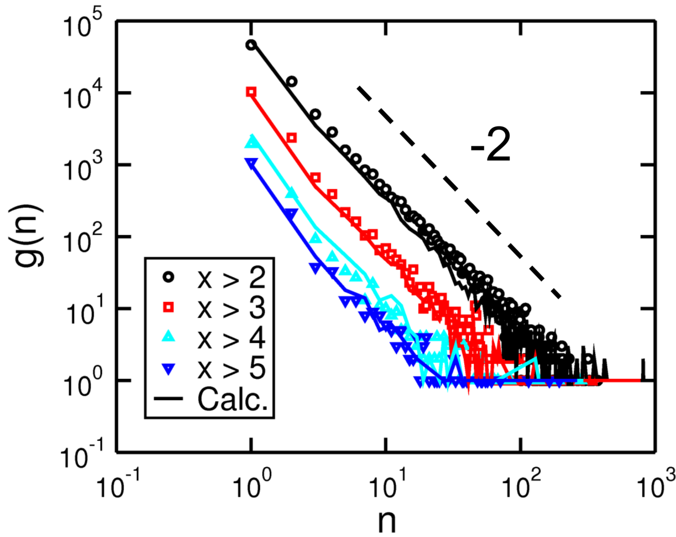

Fig. 7. Measured and calculated $g(n)$ for step amplitude x > 2, 3, 4, 5 (also including x < 1/2, 1/3, 1/4 and 1/5, respectively). The slope equal to -2 is consistent with an interrupted RTN with distribution $g(t_{on}) \sim {t_{on}}^{-2}$ of active (ON) times.

RW event frequency can be explained by a stabilization of defects contributing to the conductive path in the HRS after reset, possibly due to mechanical stress relaxation [16] and/or electrolyte structural relaxation [17]. After the initial decay, $g(t)$ stabilizes to an almost constant value, where the main contribution is due to intermittent RTN which is active only during times t_{on} as shown in Fig. 2. The RTN activity times t_{on} are almost uniformly distributed in time, thus accounting for the constant $g(t)$ at long times in Fig. 6.

Fig. 7 shows the extracted $g(n)$ for relative steps x > 2, 3, 4, 5. Each distribution also includes normalized steps lower than 1/2, 1/3, etc., as in Fig. 6. The distributions show a sharp decrease of $g(n)$ with n for all threshold values of x, thus revealing that the number of cells with a high activity of random resistance changes are only a small fraction of the array. From Fig. 7, for instance, less than 10 cells display 100 events with x > 2 or x < 1/2, or 10 events with x > 5 or x < 1/5. Relatively long repetitions of step events can be attributed to RTN taking place across a significant fraction of the experiment, which includes a maximum of 10^3 measurements of R. Note that the integral of $g(n)$ for x > 2 in Fig. 7, is 8x10^4, which is a relatively small fraction (about 15%) of the 0.5 Mb sub-array considered in our experiment. Thus we conclude that most of the cells (about 5/6) only display minor steps or no steps at all during the experiment. Therefore, both $g(t)$ and $g(n)$ represent the behavior of the cells in the distribution tail.

The step number distribution $g(n)$ mainly includes RTN fluctuations giving rise to a relatively large number of steps. Defining τ as the average transition time of RTN fluctuations, the number of steps n can be obtained as $n = t_{on}/\tau$, where t_{on} is the activity time of RTN. The extracted τ is generally 700 s, thus close to the sampling time since RTN is generally faster than the sampling rate in the experiment. Therefore, $g(t_{on})$ is proportional to $g(n)$, thus showing a -2 slope as in Fig. 7. We thus conclude that interrupted RTN fluctuations with relatively short t_{on} and displaying only few bistable switching events have a higher probability in RRAM cells.

V. Statistical model

We developed a statistical Monte-Carlo model to predict the resistance broadening within a RRAM array, based on both RW and RTN contributions. To account for the observed time decay of RW events in Figs. 4 and 6, RW was described by the defect structural relaxation model in Fig. 8 [13], [18]. After the reset operation, defects along the conduction path in HRS relax and stabilize according to the sequence of energy barriers E_{RW} in Fig. 8a. Here, each transition corresponds to a defect annihilation or relaxation, resulting in the conductive path switching to a new value of resistance. The characteristic transition time t_{RW} for RW steps can be calculated by [11]:

$$\tau_{RW} = \tau_0 e^{\frac{E_{RW}}{kT}}, \tag{3}$$

where τ_0 is a constant, k is the Boltzmann constant and T is the local temperature. Based on Eq. (3), defects with the lowest E_{RW} undergo annihilation/relaxation first, followed by other defects with increasing E_{RW}. The time distribution of events $g(t_{RW})$ in Fig. 6 is thus dictated by the E_{RW} distribution $g(E_{RW})$ according to:

$$g(t_{RW}) = g(E_{RW})\frac{dE_{RW}}{dt_{RW}}. \tag{4}$$

Assuming a constant energy distribution $g(E_{RW}) = A$ as in Fig. 8b, Eq. (4) yields:

$$g(t_{RW}) = \frac{AkT}{t_{RW}}, \tag{5}$$

which accounts for the slope -1 of $g(t)$ in Fig. 6. Fig. 8c shows the calculated $g(t_{RW})$ as a function of time for a Monte

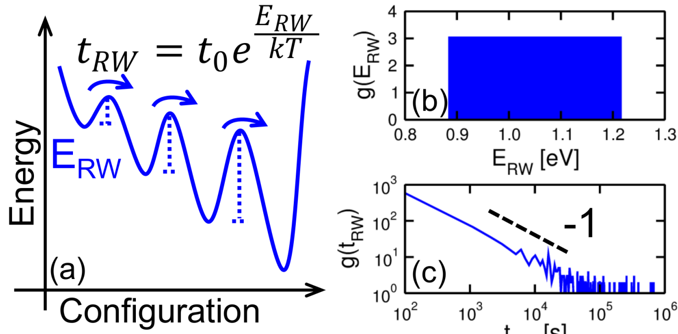

Fig. 8. Energy relaxation model for RW based on distributed energy barriers E_{RW} (a), calculated distribution of E_{RW} (b) and resulting distribution of RW time $g(t_{RW})$ (c). A uniform E_{RW} distribution (b) leads to a power-law distribution $g(t_{RW}) \sim t_{RW}{}^{-1}$ (c).

Carlo simulation. To calculate the distribution, 10^3 random values of E_{RW} where generated and the corresponding times were computed by Eq. (3), allowing to reproduce the behavior $g(t) \propto t^{-1}$. In the model, random values of E_{RW} were generated according to the uniform distribution between 0.89 and 1.22 eV in Fig. 8b, while τ_0 was assumed equal to 10^{-13} s. The relative amplitude of RW steps was assumed consistent with a power distribution $g(x) \propto (x)^{\pm 4.5}$.

Intermittent RTN can be explained by a bistable defect which fluctuates between an inactive, OFF state, and an active ON state characterized by RTN bistability, as schematically shown in Fig. 9a. We assume that the RTN defect changes its charge state in the ON state, between neutral (0) and negative (-1), thus causing a RTN modulation of the resistance along the conductive path of HRS as shown in Fig. 9b [13]. In the model, we assumed that the distribution of ON times $g(t_{on})$ follows a power law, namely $g(t_{on}) \propto t_{on}^{-2}$ while the relative amplitude of RTN steps is assumed equal to the distribution of RW steps amplitude $g(x) \propto (x)^{\pm 4.5}$. The initial times for RTN fluctuation were taken randomly within the simulation time, from 0 to 7x10^5 s.

Finally, the distributions of the number of defects $g(n_D)$ responsible for RW and RTN were studied directly on data in Fig. 10. These were evaluated by counting the number of RW events and RTN sequences in each cell, allowing to separately obtain the distributions $g(n_D)$ for RW and RTN. Both distributions show a Poisson statistics with an average number of traps of 3 defects per cell for RW and 0.8 defects per cell for RTN. Based on these results, we assumed Poisson distributed defects in the array cells, as shown by the calculated $g(n_D)$ in Fig. 10 in good agreement with data. For instance, extracting 3 traps for RW means that the calculated cell resistance shows 3 RW steps, while extracting 3 RTN traps leads to three independent RTN fluctuators, hence 2^3 = 8 resistance levels.

VI. Calculated Results

We performed Monte Carlo simulations based on the statistical model in the previous section. In the simulations, random number of defects were generated for RW and RTN according

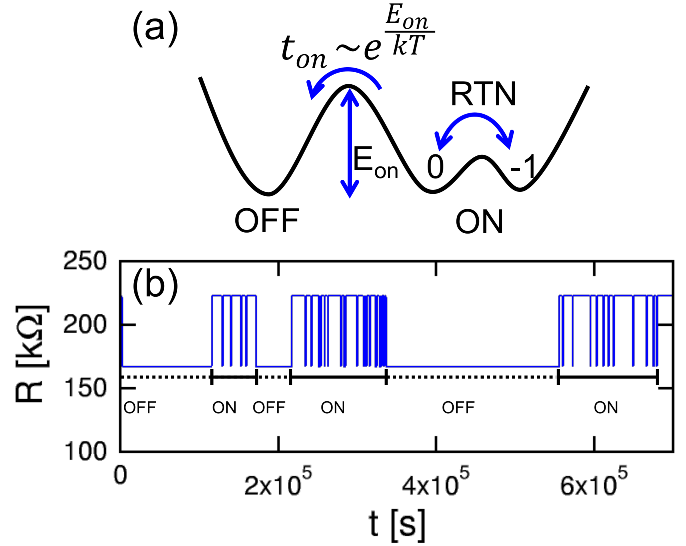

Fig. 9. Energy profile for intermittent RTN with OFF (inactive) and ON (active) states (a), and experimentally observed intermittent RTN (b).

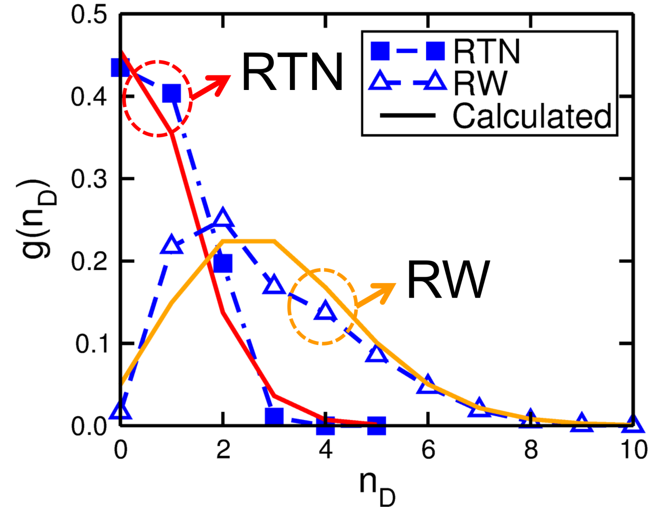

Fig. 10. Measured and calculated $g(n_D)$ of the number of RW/RTN defects per cell, indicating a Poisson distribution shape.

to $g(n_D)$ in Fig. 10, then RW defects were assigned an energy E_{RW} according to Figs. 8b. The active and starting times for RTN defects were also extracted randomly. RW and RTN amplitudes were generated randomly based on Fig. 4. The initial resistance was chosen randomly from a lognormal distribution centered on the median value of the data array, 133 kΩ. Fig. 1a shows the calculated CDF of resistance at increasing time, showing negligible broadening with time. Fig. 1b shows the calculated CDF for the normalized resistance $R(t)/R_0$, indicating a close agreement with data which supports the Monte Carlo statistical model as an accurate tool for predicting the distribution broadening in the array. The broadening is initially large due to the RW contribution, then, for increasing times, broadening is slower because of decaying RW phenomena and dominant role of intermittent RTN. The calculated $g(x)$ is reported in Fig. 4 at increasing

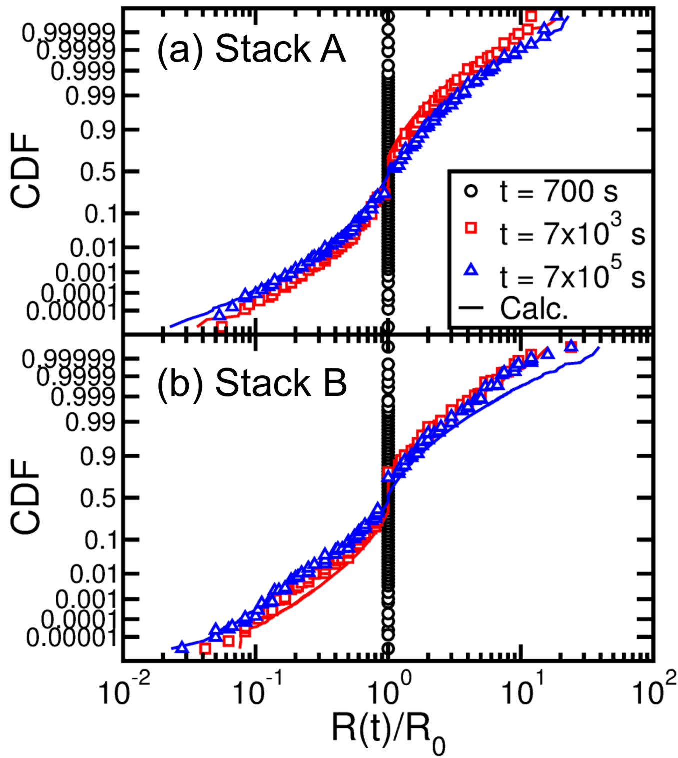

Fig. 11. Measured and calculated distributions of R/R_0 at increasing times for stacks A (a) and B (b).

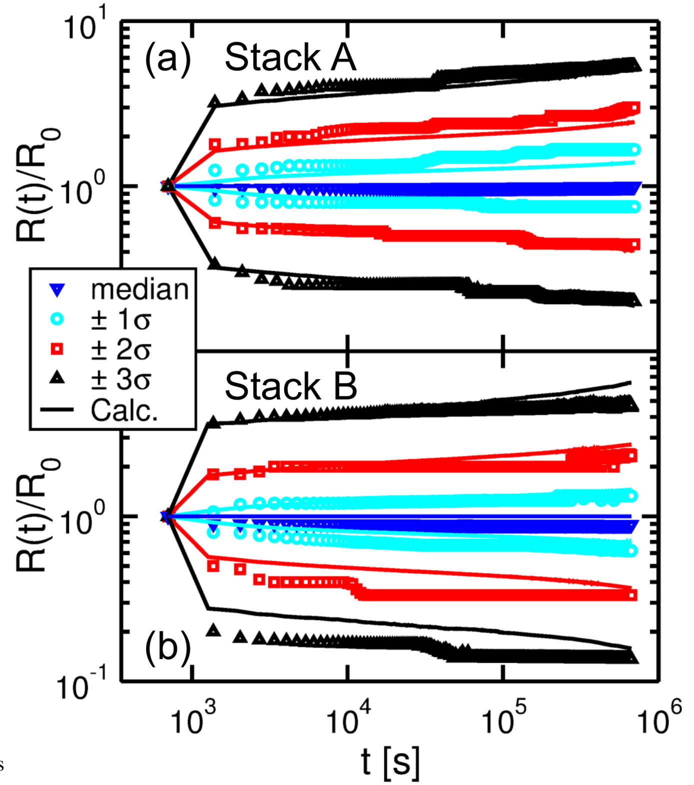

Fig. 12. Measured and calculated $R(t)/R_0$ at increasing cumulative probability, namely median value (50% percentile), $\pm\sigma$ (68.3%), $\pm 2\sigma$ (95.5%), $\pm 3\sigma$ (99.7%) for stacks A (a) and B (b). Note the symmetric broadening taking place mostly within the first 2 measurements.

time, highlighting the decay of $g(x)$ with time due to the energy distribution of RW in Fig. 8b. The time decay of RW is also seen in Fig. 6 showing the calculated $g(t)$ at variable step amplitude, where the initial decay is due to RW while the constant plateau corresponds to the stationary RTN contribution. Finally, Fig. 7 shows the calculated $g(n)$, where the slope -2 is a consequence of $n = t_{on}/\tau$ and $g(t_{on}) \propto t_{on}^{-2}$. In the calculations, the average RTN switching time τ was assumed equal to 860 s thus close to the sampling time in the experiment. Overall, the agreement between the Monte Carlo simulations and data is excellent, which further evidence that our model of RW and RTN fluctuations is physically sound.

To investigate the material dependence of distribution broadening, we compared 2 different RRAM stacks were compared, namely stacks A and B. Fig. 11 shows the measured and calculated CDF of normalized resistance for stack A, (same data as in Fig. 1b) and stack B. The distributions for the 2 RRAM materials show negligible differences except for slightly asymmetric tails for stack B. This is due to a minor drift of the resistance to lower values resulting in a larger tail at $R(t)/R_0 < 1$. Drift can be attributed to cycle-to-cycle variations of HRS stability, which was sometimes also observed in stack A. The calculated results show a good agreement with data for both RRAM materials. To better highlight the time evolution of broadening, Fig. 12 shows the measured and calculated $R(t)/R_0$ in correspondence of increasing cumulative probability, namely 50% (median value), at $\pm\sigma$ (corresponding to 50% $\pm$ 9%), at $\pm 2\sigma$ (corresponding to to 50% $\pm$ 22.75%) and $\pm 3\sigma$ (corresponding to to 50% $\pm$ 24.85%), for stacks A

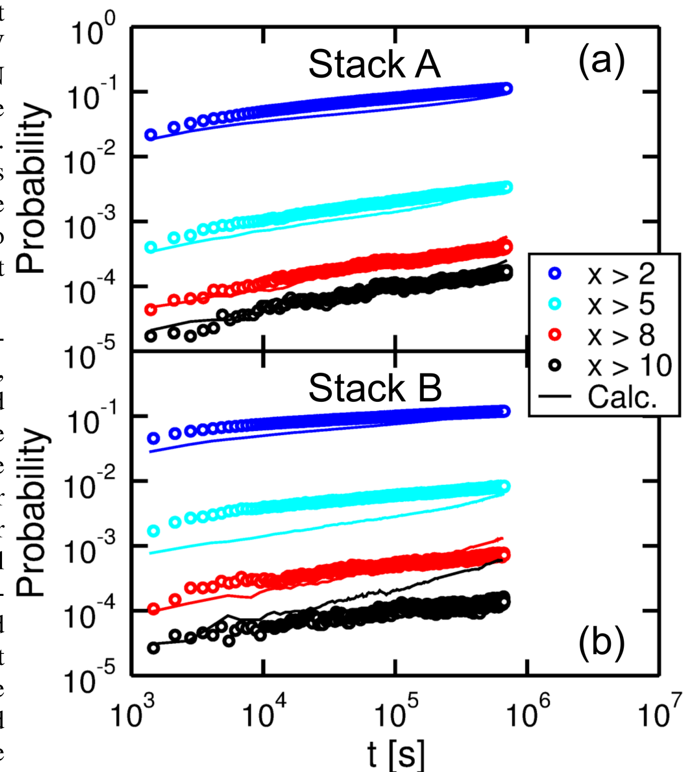

Fig. 13. Measured and calculated probability for the resistance to exceed a certain step amplitude x (or $1/x$) in Fig. 11 for stacks A (a) and B (b).

(a) and B (b). For stack A, the tails are symmetrical and the median is constant, revealing no resistance drift, while stack B shows a minor drift of the median towards lower resistance causing an asymmetry of the distribution tails. Note that most of the broadening takes place in the first time step, namely between 700 s and 1400 s in our experiment, which is due in part to the time-decaying behavior of RW in Figs. 4 and 6. In fact, since more fluctuations take place at relatively early times after reset, a large broadening occurs in the same time scale. Finally, Fig. 13 shows the probability for a cell to fall beyond a relative change of resistance larger than 2, 5, 8 or 10 in the distributions of Fig. 12, for stack A (a) and B (b). For increasing times, the probability increases due to resistance broadening. Also in this case the model accurately accounts for data for both stacks. Data confirms that the observed broadening is a universal feature with negligible dependence on RRAM material, and that our model accounts closely for all statistical features of noise, thanks to a physically-based description of RW and RTN fluctuations.

VII. Conclusions

We addressed the statistics of resistance fluctuations in RRAM arrays. We found 2 main contributions to large resistance fluctuations, namely RW and intermittent RTN. We provide evidence for time-decaying RW, which we explain by structural or mechanical stabilization of defects in the conductive path of the HRS after reset. Intermittent RTN is explained by activation/deactivation of bistable defects at the conductive path. Based on this physical insight into fluctuations, we developed a Monte-Carlo statistical model which accounts for the statistics of resistance broadening as a function of time. The model thus provides a physics-based accurate tool for predicting the distribution broadening of RRAM resistance in large arrays.

References

[1] S. Ambrogio, S. Balatti, V. McCaffrey, D. Wang, and D. Ielmini, "Noise-induced resistance broadening in resistive switching memory (RRAM) - Part I: Intrinsic cell behavior," *IEEE Trans. Electron Devices*, vol. Submitted.

[2] H.-S. P. Wong, H.-Y. Lee, S. Yu, Y.-S. Chen, Y. Wu, P.-S. Chen, B. Lee, F. T. Chen, and M.-J. Tsai, "Metal-oxide RRAM," *Proc. IEEE*, vol. 100, no. 6, pp. 1951–1970, 2012.

[3] M. Kozicki, C. Gopalan, M. Balakrishnan, and M. M. Mitkova, "A low-power nonvolatile switching element based on copper-tungsten oxide solid electrolyte," *IEEE Transactions on Nanotech.*, vol. 5, no. 5, pp. 535–544, 2006.

[4] I. Valov, R. Waser, J. Jameson, and M. Kozicki, "Electrochemical metallization memories–fundamentals, applications, prospects," *Nanotech.*, vol. 22, p. 254003, 2011.

[5] J. Jameson, P. Blanchard, C. Cheng, J. Dinh, A. Gallo, V. Gopalakrishnan, C. Gopalan, B. Guichet, S. Hsu, D. Kamalanathan, D. Kim, F. Koushan, M. Kwan, K. Law, D. Lewis, Y. Ma, V. McCaffrey, S. Park, S. Puthenthermadam, E. Runnion, J. Sanchez, J. Shields, K. Tsai, A. Tysdal, D. Wang, R. Williams, M. Kozicki, J. Wang, V. Gopinath, S. Hollmer, and M. V. Buskirk, "Conductive-bridge memory (CBRAM) with excellent high-temperature retention," *IEDM Tech Dig.*, pp. 30.1.1–30.1.4, 2013.

[6] H. Y. Lee, P. S. Chen, T. Y. Wu, Y. S. Chen, C. C. Wang, P. J. Tzeng, C. H. Lin, F. Chen, C. H. Lien, and M.-J. Tsai, "Low power and high speed bipolar switching with a thin reactive Ti buffer layer in robust HfO_2 based RRAM," *IEDM Tech. Dig.*, pp. 297–300, 2008.

[7] H. Lee, Y.-S. Chen, P. Chen, P. Gu, Y. Hsu, S. Wang, W. Liu, C. Tsai, S. Sheu, P.-C. Chiang, W. Lin, C.-H. Lin, W.-S. Chen, F. Chen, C. Lien, and M. Tsai, "Evidence and solution of over-RESET problem for HfO_x based resistive memory with sub-ns switching speed and high endurance," *IEDM Tech. Dig.*, pp. 460–463, 2010.

[8] M. D. Pickett and R. S. Williams, "Sub-100 fJ and sub-nanosecond thermally driven threshold switching in niobium oxide crosspoint nanodevices," *Nanotechnology*, vol. 23, p. 215202, 2012.

[9] J. Yang, M.-X. Zhang, J. Strachan, F. Miao, M. Pickett, R. Kelley, G. Medeiros-Ribeiro, and R. Williams, "High switching endurance in TaO_x memristive devices," *Appl. Phys. Lett.*, vol. 97, p. 232102, 2010.

[10] M.-J. Lee, C. Lee, D. Lee, S. Lee, M. Chang, J. Hur, Y.-B. Kim, C.-J. Kim, D. Seo, S.Seo, U.-I. Chung, I.-K. Yoo, and K. Kim, "A fast, high-endurance and scalable non-volatile memory device made from asymmetric $\mathrm{Ta_2O_{5-x}}$=$\mathrm{TaO_{2-x}}$ bilayer structures," *Nat. Mat.*, vol. 10, pp. 625–630, 2011.

[11] S. Ambrogio, S. Balatti, V. McCaffrey, D. Wang, and D. Ielmini, "Impact of low-frequency noise on read distributions of resistive switching memory (RRAM)," *IEDM Tech. Dig.*, pp. 1–4, 2014.

[12] D. Ielmini, F. Nardi, and C. Cagli, "Resistance-dependent amplitude of random telegraph-signal noise in resistive switching memories," *Appl. Phys. Lett.*, vol. 96, no. 5, p. 053503, 2010.

[13] S. Ambrogio, S. Balatti, A. Cubeta, A. Calderoni, N. Ramaswamy, and D. Ielmini, "Statistical fluctuations in HfO_x resistive-switching memory (RRAM): Part II - Random telegraph noise," *IEEE Trans. Electron Devices*, vol. 61, no. 8, pp. 2920–2927, 2014.

[14] Z. Fang, H. Y. Yu, W. J. Fan, G. Ghibaudo, J. Buckley, B. DeSalvo, X. Li, X. P. Wang, G. Q. Lo, and D. L. Kwong, "Current conduction model for oxide-based resistive random access memory verified by low-frequency noise analysis," *IEEE Trans. Electron Devices*, vol. 60, no. 3, pp. 1272–1275, 2013.

[15] S. Ambrogio, S. Balatti, A. Cubeta, A. Calderoni, N. Ramaswamy, and D. Ielmini, "Statistical fluctuations in HfO_x resistive-switching memory (RRAM): Part I - Set/Reset variability," *IEEE Trans. Electron Devices*, vol. 61, no. 8, pp. 2912–2919, 2014.

[16] S. Ambrogio, S. Balatti, S. Choi, and D. Ielmini, "Impact of the mechanical stress on switching characteristics of electrochemical resistive memory," *Adv. Mat.*, vol. 26, no. 23, p. 3885, 2014.

[17] S. Choi, S. Balatti, F. Nardi, and D. Ielmini, "Size-dependent drift of resistance due to surface defect relaxation in conductive-bridge memory," *Electron Device Letters, IEEE*, vol. 33, no. 8, pp. 1189–1191, 2012.

[18] D. Ielmini, S. Lavizzari, D. Sharma, and A. L. Lacaita, "Temperature acceleration of structural relaxation in $\mathrm{Ge_2Sb_2Te_5}$," *Appl. Phys. Lett.*, vol. 92, p. 193511, 2008.